

Spectral effects in quantum teleportation

Travis S. Humble* and Warren P. Grice†

Center for Engineering Science Advanced Research, Computer Science and Mathematics Division, Oak Ridge National Laboratory, Oak Ridge, Tennessee 37831-6016, USA

(Received 14 November 2006; published 8 February 2007)

We use a multimode description of polarization-encoded qubits to analyze the quantum teleportation protocol. Specifically, we investigate how the teleportation fidelity depends on the spectral correlations inherent to polarization-entangled photons generated by type-II spontaneous parametric down conversion. We find that the maximal obtainable fidelity depends on the spectral entanglement carried by the joint probability amplitude, a result which we quantify for the case of a joint spectrum approximated by a correlated Gaussian function. We contrast these results with a similar analysis of the visibility obtained in a polarization-correlation experiment.

DOI: 10.1103/PhysRevA.75.022307

PACS number(s): 03.67.Mn, 42.50.Dv

I. INTRODUCTION

Quantum teleportation [1] is a basic building block in many quantum communication and quantum computation protocols [2]. In its simplest form, the quantum teleportation protocol transfers a qubit of information encoded originally in the two-level structure of particle 1 as $|\psi_1\rangle = a|\uparrow_1\rangle + b|\downarrow_1\rangle$ to a remote particle 3 comprising half of the entangled Bell state $|\varphi_{23}\rangle = (|\uparrow_2, \downarrow_3\rangle + |\downarrow_2, \uparrow_3\rangle)/\sqrt{2}$. Upon performing a Bell-state measurement on particles 1 and 2, the state of particle 3 relates to the original qubit by some unitary transformation that depends on the measurement outcome. The outcome is communicated to the recipient of particle 3, who then applies the appropriate transformation to recover the state of the original qubit [1]. This seemingly simple protocol underlies applications such as quantum repeaters and relays [3–5], quantum memories [6], and forms of efficient linear optical quantum computing [7].

Many experimental implementations of quantum teleportation use the orthogonal polarization states of a photon as a model two-level system for encoding qubits of information [3–13]. These efforts to teleport polarization-encoded qubits are facilitated by the relatively bright sources of polarization-entangled photons obtainable from spontaneous parametric down-conversion (SPDC) [14,15], as well as the ease with which a partial Bell-state measurement can be implemented using linear optics and detectors [16]; see Fig. 1. Using these techniques, teleportation fidelities as high as 92% have been reported [11].

Although a simplified two-level description of light quanta is often sufficient for theoretical exploration and proof-of-principle experiments, the additional degrees of freedom inherent to a photon should also contribute to the overall fidelity of teleportation. Indeed, previous experimental setups have prudently filtered the spatial and spectral degrees of freedom in order to ensure high fidelity teleportation. But such filtering comes at the cost of significantly reduced (coincidence) count rates. Refraining from the use of spectral and spatial filtering may greatly enhance the rate and

efficiency with which qubits are teleported, but only if it is possible to simultaneously maintain maximal teleportation fidelity.

An understanding of the quantum teleportation protocol in a multimode context requires nontrivial analogs of the usual polarization-encoded qubits. In particular, SPDC is known to produce a biphoton state with a joint spectral probability amplitude of innately broad bandwidth. Moreover, the joint spectral amplitude of the photon pair is typically strongly entangled with respect to frequency because of the conservation of energy requirements mediating the down-conversion process. For type-II SPDC, the spectral properties of the individual photons typically correlate with the polarization degree of freedom [17,18]. However, it is also possible to generate a polarization entangled state in which the spectral properties of the photons correlate with their path, rather than their polarization [19]. Additional sources of distinguishing information may be found in correlations between the spectra and the other degrees of freedom. These aspects of “realistic” polarization-entangled photons complicate the multimode extension of the quantum teleportation protocol implemented in previous experiments.

The distinguishing information inherent to the biphoton states generated by SPDC has been analyzed previously us-

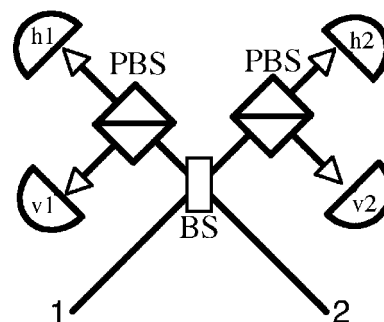


FIG. 1. A sketch of the partial Bell-state measurement device using linear optics and detectors; cf. Ref [16]. Photons 1 and 2 interfere at a 50:50 beam splitter (BS) whose output ports direct into polarizing beam splitters (PBS). The PBS transmits (reflects) horizontally (vertically) polarized photons into subsequent detectors. Coincidence counts between pairs of detectors, e.g., h1 and v1, signal that a Bell-state measurement has occurred.

*Email address: humblets@ornl.gov

†Email address: gricewp@ornl.gov

ing fourth-order interference experiments [17,18,20–22]. In those earlier experiments, the effects of spectral correlations on polarization entanglement were identified in terms of the reduced visibility in a Hong-Ou-Mandel interferometer [23]. Specifically, for the case of type-II SPDC, submaximal interference at a 50:50 beam splitter resulted from the distinguishable joint spectra that characterized the different polarization amplitudes comprising the entangled state. Theoretical and experimental analyses of the joint spatial amplitudes produced by SPDC have led to similar results [24,25].

Given the prominent use of SPDC to generate polarization-entangled photons for demonstrations of quantum information protocols, the role that distinguishable spectral and spatial amplitudes play in specific protocols is of increasing interest. Previously, U'Ren *et al.* analyzed how the form of the joint spectral amplitudes affect the detection statistics in the Braunstein-Mann Bell-state analyzer and the two-photon polarization-correlation measurements [26]. Specifically, they found that the polarization-correlation visibility is maximal when spectral differences between the photons correlate with path, while coincidences in the Bell-state analyzer are optimized when spectral differences correlate with polarization. Kim and Grice reported similar results in their analysis of the optical Bell-state analyzer [27]. Recently, Rohde and Ralph have incorporated the effects of broad bandwidth single photons in a controlled-NOT gate and subsequently showed that the temporal distinguishability between the photons and the finite detector resolution may also reduce the gate fidelity and success probability [28]. Rohde *et al.* investigated more general linear optical circuits in a similar context, observing that the undesirable effects of mode distinguishability are perhaps best mitigated through the use of broad bandwidths, most notably those of Gaussian form [29].

In this paper, we investigate how the aforementioned spectral correlations influence teleporting the polarization state of a photon. We begin in Sec. II with a multimode description of the polarization-entangled photon pairs that uses a correlated Gaussian approximation for the joint spectral amplitude generated by type-II SPDC. An analysis of the polarization-correlation experiment and the role that the shape of the joint spectral amplitude plays in determining polarization entanglement is presented in Sec. III. In Sec. IV, we use similar multimode expressions for the polarization-encoded qubits employed in the quantum teleportation protocol, and we derive the corresponding fidelity of teleportation. We determine the conditions necessary for maximizing teleportation fidelity when the photon pairs are spectrally entangled, and we quantify the maximal obtainable fidelity. We conclude our discussion in Sec. V.

II. MULTIMODE POLARIZATION-ENTANGLED PHOTON PAIRS

As an extension of the single-mode polarization-entangled biphoton state of photons 2 and 3, we consider the multimode analog

$$|\varphi_{23}\rangle = \frac{1}{\sqrt{2}} \int d\omega \int d\omega' [f(\omega, \omega') |h_2(\omega), v_3(\omega')\rangle + g(\omega, \omega') |v_2(\omega), h_3(\omega')\rangle], \quad (1)$$

where $f(\omega, \omega')$ and $g(\omega, \omega')$ are the joint spectral probability amplitudes corresponding to the polarization states $|h_2(\omega), v_3(\omega')\rangle$ and $|v_2(\omega), h_3(\omega')\rangle$.¹ We denote the horizontally and vertically polarized modes of photon j at frequency ω as $|h_j(\omega)\rangle = h_j^\dagger(\omega)|\text{vac}\rangle$ and $|v_j(\omega)\rangle = v_j^\dagger(\omega)|\text{vac}\rangle$, respectively, and the tensor product $|h_j(\omega)\rangle \otimes |v_k(\omega')\rangle$ as $|h_j(\omega), v_k(\omega')\rangle$. We assume Eq. (1) is normalized and that

$$\int d\omega \int d\omega' |f(\omega, \omega')|^2 = \int d\omega \int d\omega' |g(\omega, \omega')|^2 = 1, \quad (2)$$

i.e., probability is equally partitioned between the two joint polarization amplitudes.

We first consider the case that

$$g(\omega, \omega') = f(\omega', \omega), \quad (3)$$

which occurs, for example, when the photons originate from a type-II crystal in the cross-ring configuration [14]. Physically, the relationship between f and g given by Eq. (3) describes individual photons whose spectral properties correlate with the polarization degree of freedom, i.e.,

$$|\varphi_{23}^{\text{pol.}}\rangle = \frac{1}{\sqrt{2}} \int d\omega \int d\omega' f(\omega, \omega') [|h_2(\omega), v_3(\omega')\rangle + |v_2(\omega'), h_3(\omega)\rangle]. \quad (4)$$

In general, Eq. (4) cannot be factored with respect to the spectral and polarization degrees of freedom. When the marginal spectra of the photons are distinct, this inseparability serves as a source of distinguishing information. In contrast, when the joint spectral amplitudes are equivalent,

$$g(\omega, \omega') = f(\omega, \omega'), \quad (5)$$

the biphoton state is given by

$$|\varphi_{23}^{\text{path}}\rangle = \frac{1}{\sqrt{2}} \int d\omega_2 \int d\omega_3 f(\omega_2, \omega_3) [|h_2(\omega_2), v_3(\omega_3)\rangle + |v_2(\omega_2), h_3(\omega_3)\rangle]. \quad (6)$$

In Eq. (6), individual photon properties correlate with the path taken and are decoupled from the polarization. Hence, the previous source of distinguishing information is avoided, i.e., while the photons in paths 2 and 3 may be spectrally distinguishable, these differences provide no polarization information. Biphoton states whose joint spectra satisfy Eq. (5) are generally not directly produced by type-II SPDC. However, it is possible to manipulate the output state postproduc-

¹We focus on spectral distinguishability by assuming spatial filters select the paths photons 2 and 3 travel after leaving the crystal; the transverse momenta corresponding to these directions are assumed equal in magnitude and opposite in sign, while the pump propagates in the z direction.

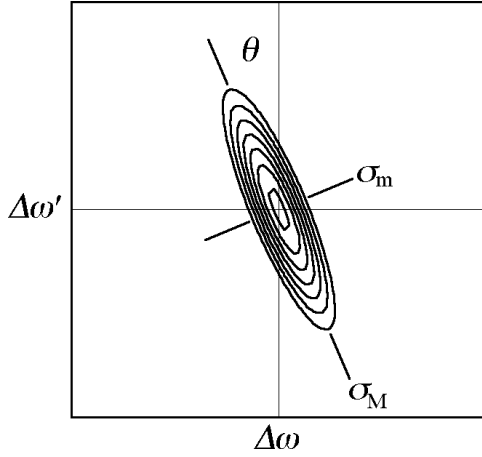


FIG. 2. A schematic drawing of the correlated Gaussian amplitude expressed in terms of the major and minor widths σ_M and σ_m , respectively, and the orientation angle θ .

tion such that Eq. (5) holds, albeit at the cost of additional optical elements [19,22,26].

In the following analysis, we invoke a Gaussian approximation for the joint spectral amplitude, the details of which are deferred to the Appendix. We express the joint spectrum in terms of a bivariate normal distribution

$$f(\Delta\omega, \Delta\omega') = N \exp \left[-\frac{1}{2(1-\rho^2)} \left(\frac{\Delta\omega^2}{\sigma^2} - \frac{2\rho\Delta\omega\Delta\omega'}{\sigma\sigma'} + \frac{\Delta\omega'^2}{\sigma'^2} \right) \right], \quad (7)$$

where $\Delta\omega$ and $\Delta\omega'$ are difference frequencies, σ and σ' are the corresponding marginal bandwidths, and $N^{-2} = \sigma\sigma'\sqrt{1-\rho^2}$. The correlation ρ ranges from +1 to -1, where positive values indicate frequencies are correlated, negative values indicate they are anticorrelated, and zero implies no correlation. Expressions for these model parameters in terms of experimental parameters are given in the Appendix.

We also make use of the diagonal representation of Eq. (7), in which the principal axes of the error ellipse have undergone a rotation through the angle θ ; see Fig. 2. In this equivalent form,

$$f(\Delta\omega, \Delta\omega') = N \exp \left[-(\Delta\omega \cos \theta + \Delta\omega' \sin \theta)^2 / 2\sigma_M^2 - (\Delta\omega' \cos \theta - \Delta\omega \sin \theta)^2 / 2\sigma_m^2 \right], \quad (8)$$

where the major and minor widths of the joint spectrum, σ_M and σ_m , respectively, are related to the marginal bandwidths by

$$\begin{aligned} \sigma^2 &= \sigma_M^2 \cos^2 \theta + \sigma_m^2 \sin^2 \theta \\ \sigma'^2 &= \sigma_m^2 \cos^2 \theta + \sigma_M^2 \sin^2 \theta. \end{aligned} \quad (9)$$

The latter satisfy the relationship $\sigma_M^2 \sigma_m^2 = \sigma^2 \sigma'^2 (1-\rho^2)$, while the angle θ is defined by

$$\tan 2\theta = \frac{2\rho\sigma\sigma'}{\sigma^2 - \sigma'^2}. \quad (10)$$

This alternate form has the benefit of providing an intuitive understanding of how changes in the model parameters affect changes in the global form of the joint spectral amplitude. For example, when $\theta=0, \pm\pi/2$, the joint spectrum is unentangled and can be factored as $f(\omega, \omega') = f_1(\omega)f_2(\omega')$, where $f_j(\omega)$ is a single-photon spectral probability amplitude.

III. POLARIZATION CORRELATIONS

Given the total density matrix $\rho_{23} = |\varphi_{23}\rangle\langle\varphi_{23}|$, the joint polarization state of photons 2 and 3 is obtained by tracing over the spectral degrees of freedom,

$$\tilde{\rho}_{23} = \text{Tr}_{\omega, \omega'}[\rho_{23}], \quad (11)$$

and is expressed in the basis $\{|h_2, v_3\rangle, |v_2, h_3\rangle\}$ as

$$\tilde{\rho}_{23} = \frac{1}{2} \begin{pmatrix} 1 & G \\ G^* & 1 \end{pmatrix}. \quad (12)$$

The quantity

$$G = \int d\omega \int d\omega' f(\omega, \omega') g(\omega, \omega')^* \quad (13)$$

measures the interference between the joint spectral amplitudes and ranges from 0 (completely distinguishable) to 1 (indistinguishable).

As a quantitative measure of the polarization entanglement, we use the concurrence C , which is directly related to the entanglement of formation [31]. For the case of the discrete bipartite density matrix $\tilde{\rho}_{23}$, the concurrence is given by

$$C = \max\{0, \lambda_1 - \lambda_2 - \lambda_3 - \lambda_4\}, \quad (14)$$

where the λ_i 's (with $\lambda_1 \geq \lambda_2 \geq \lambda_3 \geq \lambda_4$) are the square roots of the eigenvalues of the Hermitian matrix

$$\tilde{\rho}_{23}(\sigma_{2y} \otimes \sigma_{3y}) \tilde{\rho}_{23}^*(\sigma_{2y} \otimes \sigma_{3y}). \quad (15)$$

In this example, the Pauli single-qubit operators σ_{2y} and σ_{3y} are expressed as $\sigma_{2y} = i|v_2\rangle\langle h_2| - i|h_2\rangle\langle v_2|$ and $\sigma_{3y} = i|v_3\rangle\langle h_3| - i|h_3\rangle\langle v_3|$. Diagonalization of Eq. (15) yields

$$\begin{aligned} \lambda_1 &= \frac{1+|G|}{2}, \\ \lambda_2 &= \frac{1-|G|}{2}, \end{aligned} \quad (16)$$

and $\lambda_3 = \lambda_4 = 0$. It then follows from Eq. (14) that the concurrence is $C = |G|$, and, consequently, we may take $|G|$ as a measure of the entanglement in its own right [31].

Experimentally, polarization entanglement is often quantified by the visibility in a polarization-correlation experiment [14,15]. For a pair of polarizers defined by the output modes $a_j^\dagger = h_j^\dagger \cos \theta_j + v_j^\dagger \sin \theta_j$ ($j=2,3$), the conditional probability for coincidence detection behind both polarizers is [26,27] (assuming constant detector efficiencies)

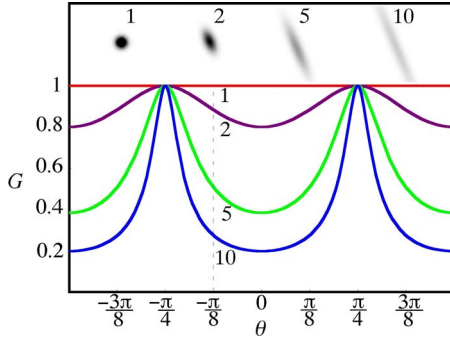


FIG. 3. (Color online) The concurrence (or visibility) for the case $f(\omega, \omega') = g(\omega', \omega)$ plotted as a function of θ . Each curve is labeled by the value of the ratio σ_M/σ_m : 1 (red), 2 (brown), 5 (green), and 10 (blue) and is exemplified along the upper border by a plot of the corresponding joint spectrum when $\theta = -\pi/8$.

$$P(\theta_3|\theta_2) = \int d\omega \int d\omega' |f(\omega, \omega') \cos \theta_2 \sin \theta_3 + g(\omega, \omega') \sin \theta_2 \cos \theta_3|^2. \quad (17)$$

The visibility of the polarization-correlation experiment in the diagonal ($\pm 45^\circ$) basis is subsequently defined as

$$V = \frac{P(\pi/4|\pi/4) - P(\pi/4|3\pi/4)}{P(\pi/4|\pi/4) + P(\pi/4|3\pi/4)} = \text{Re } G. \quad (18)$$

For our real-valued approximation to the joint spectral amplitude, this definition of the visibility coincides with the concurrence.

Using the approximate amplitude given by Eq. (7), a straightforward calculation of the overlap G when the spectral differences correlate with polarization, i.e., when Eq. (3) holds, yields

$$G = \sqrt{\frac{4\sigma^2\sigma'^2(1-\rho^2)}{(\sigma^2 + \sigma'^2)^2 - 4\sigma^2\sigma'^2\rho^2}}. \quad (19)$$

In the absence of spectral correlations, $|\rho| = 0$ and we find $G = 2\sigma\sigma' / (\sigma^2 + \sigma'^2)$, which approaches unity as the marginal bandwidths become equal. In the other extreme, G vanishes as $|\rho|$ approaches 1 because the increasing frequency entanglement between the photons leads to greater spectral distinguishability.

We can also express the overlap G using Eqs. (9) and (10) as

$$G = \frac{2\sigma_M\sigma_m}{\sqrt{(\sigma_M^2 + \sigma_m^2)^2 - (\sigma_M^2 - \sigma_m^2)^2 \sin^2 2\theta}}. \quad (20)$$

This model for both the concurrence and the visibility is plotted in Fig. 3 as a function of θ with various integral values of the aspect ratio $a = \sigma_M/\sigma_m$. As shown, the concurrence is maximal for $a = 1$ because the joint spectral amplitude is circularly symmetric and the individual photon properties are independent of θ . For $a \neq 1$, maxima in the visibility occur at $\theta = \pm \pi/4$. At these orientations, the individual photons are spectrally indistinguishable despite the strong frequency correlations, e.g., $|\rho| = (a^2 - 1)/(a^2 + 1)$. In

contrast, minima in the concurrence occur at $\theta = 0, \pm \pi/2$. Although the joint amplitudes are separable with respect to frequency, the individual photon properties are more distinguishable with larger a .

Different behavior is observed when the spectral differences between the photons correlate with path and $f(\omega, \omega') = g(\omega, \omega')$. For this case, the spectral and polarization degrees of freedom are decoupled and the entanglement is always maximal, independent of the spectral entanglement between the photons.

IV. MULTIMODE ANALYSIS OF QUANTUM TELEPORTATION

Our analysis in Sec. III investigated how spectral distinguishability reduces polarization entanglement. In this section, we consider the quantum teleportation protocol in a similar context. We take the normalized state of photon 1 as a multimode analog of the qubit, i.e.,

$$|\psi_1\rangle = \int s(\omega)[\alpha|h_1(\omega)\rangle + \beta|v_1(\omega)\rangle]d\omega, \quad (21)$$

where $s(\omega)$ is the spectral amplitude and $|\alpha|^2 + |\beta|^2 = 1$. As before, the polarization state is defined by tracing over the spectral degrees of freedom, $\tilde{\rho}_1 = \text{Tr}_\omega[\rho_1]$ with $\rho_1 = |\psi_1\rangle\langle\psi_1|$. We use the multimode analog of the polarization-entangled state for photons 2 and 3 given by Eq. (1).

In a typical quantum teleportation experiment using polarization-encoded qubits, photons 1 and 2 are incident on the input ports of a 50:50 beam splitter with the subsequent output analyzed using a pair of polarizing beam splitters and four detectors [16]; see Fig. 1. The projection of photons 1 and 2 into two of the four polarization-entangled Bell states is identified based on the signature of the detectors firing (the other two Bell states being indistinguishable with this linear scheme [32]).

To model the partial Bell-state measurement technique, we describe the output of the 50:50 beam splitter by the Heisenberg equations

$$B^\dagger h_1(\omega)B = [h_2(\omega) + ih_1(\omega)]/\sqrt{2}$$

$$B^\dagger h_2(\omega)B = [h_2(\omega) - ih_1(\omega)]/\sqrt{2}, \quad (22)$$

where B is a unitary operator and similar equations hold for $v_{1,2}(\omega)$. Following the beam splitter, detection of photons 1 and 2 is modeled by the operator, e.g.,

$$\Pi(h_1, v_1) = \int \varepsilon_{h_1}(\omega)|h_1(\omega)\rangle\langle h_1(\omega)|d\omega \otimes \int \varepsilon_{v_1}(\omega')|v_1(\omega')\rangle\langle v_1(\omega')|d\omega', \quad (23)$$

which accounts for coincidences between detectors h_1 and v_1 . In Eq. (23), the integrals over frequencies account for the spectral bandwidths of the incident photons while the detector efficiencies $\varepsilon_{h_1}(\omega)$ and $\varepsilon_{v_1}(\omega)$ account for any spectral filtering at detectors h_1 and v_1 , respectively. Here we neglect the effects of the latter, and unit efficiencies are assumed. Other detection possibilities may be similarly modeled [33].

The unnormalized state of photon 3 following coincidences at, e.g., detectors h_1 and v_1 , is

$$\rho_3 = \text{Tr}_{12}[\Pi(h_1, v_1)B^\dagger \rho_{123}B], \quad (24)$$

where $\rho_{123} = |\Psi_{123}\rangle\langle\Psi_{123}|$ and the trace is taken over photons 1 and 2. The polarization state of photon 3 is given by the reduced density matrix $\tilde{\rho}_3 = \text{Tr}_{\omega}\rho_3$, which, following normalization and assuming constant detector efficiencies, is expressed in the h - v polarization basis as²

$$\tilde{\rho}_3 = \begin{pmatrix} |\alpha|^2 & \alpha\beta^*J \\ \alpha^*\beta J^* & |\beta|^2 \end{pmatrix}. \quad (25)$$

The overlap integral

$$J = \int d\bar{\omega} \left(\int s(\omega)f(\omega, \bar{\omega})^* d\omega \right) \left(\int s^*(\omega')g(\omega', \bar{\omega}) d\omega' \right) \quad (26)$$

accounts for spectral distinguishability of the entangled source as well as the interference between photons 1 and 2 at the beam splitter.

The fidelity of teleportation, defined as the inner product of $\tilde{\rho}_1$ and $\tilde{\rho}_3$, is

$$F = \text{Tr}[\tilde{\rho}_1\tilde{\rho}_3] = |\alpha|^4 + |\beta|^4 + 2|\alpha\beta|^2 \text{Re } J,$$

which is linear in J . As an explicit example, we consider $|\alpha|^2 = |\beta|^2 = 1/2$, for which the fidelity simplifies to

$$F = \frac{1}{2}(1 + \text{Re } J). \quad (27)$$

We now consider in more detail the behavior of J and its role in determining the fidelity of teleportation. We assume photon 1 has a Gaussian spectrum with a mean frequency of ω_0 ,

$$s(\Delta\omega) = (\pi\sigma_1^2)^{-1/4} \exp(-\Delta\omega^2/2\sigma_1^2), \quad (28)$$

where σ_1 determines the $(1/e)$ spectral bandwidth, and the joint spectral amplitude of photons 2 and 3 is given by Eqs. (7) and (8).

In our first example, we consider the spectral differences to correlate with polarization. The overlap J is calculated using Eqs. (8) and (28) and found to be

$$J_{\text{pol.}} = \frac{4\sigma_1\sigma_M\sigma_m}{\sqrt{2(\sigma_M^2 + \sigma_m^2)(\sigma_M^2 + \sigma_1^2)(\sigma_m^2 + \sigma_1^2) - (\sigma_M^2 - \sigma_m^2)^2\sigma_1^2 \sin^2 2\theta}}. \quad (29)$$

Maximization of Eq. (29) yields an optimal bandwidth for photon 1 of $\sigma_1 = \sqrt{\sigma_M\sigma_m}$ and the corresponding maximal teleportation fidelity

²Other coincidences, e.g., h_1 and v_2 , require a local unitary transformation of photon 3's polarization state in order to recover the form (25).

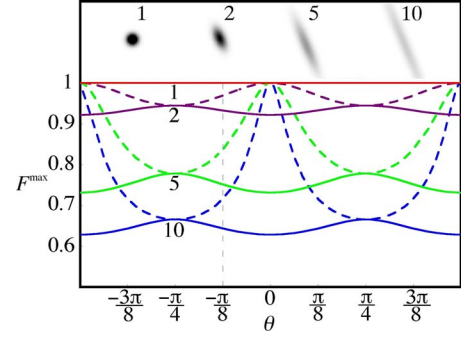


FIG. 4. (Color online) Plots of the maximal teleportation fidelities $F_{\text{pol.}}^{\text{max}}$ (solid) and $F_{\text{path}}^{\text{max}}$ (dashed) as a function of the orientation angle θ . Each curve is labeled by the value of the ratio σ_M/σ_m : 1 (red), 2 (brown), 5 (green), and 10 (blue). Each ratio is exemplified along the upper boarder by a plot of the corresponding joint spectrum when $\theta = -\pi/8$.

$$F_{\text{pol.}}^{\text{max}} = \frac{1}{2} + \frac{2\sigma_M\sigma_m}{\sqrt{2(\sigma_M^2 + \sigma_m^2)(\sigma_M + \sigma_m)^2 - (\sigma_M^2 - \sigma_m^2)^2 \sin^2 2\theta}}, \quad (30)$$

which varies sinusoidally as a function of the angle 2θ . As shown in Fig. 4, peaks in $F_{\text{pol.}}^{\text{max}}$ occur when $\theta = \pm\pi/4$. Although photons 2 and 3 have identical spectra here, the fidelity is less than unity because the spectral entanglement serves as a means for distinguishing between the photons based on color. We elucidate this point by rewriting $F_{\text{pol.}}^{\text{max}}$ in terms of the linear correlation ρ ,

$$F_{\text{pol.}}^{\text{max}} = \frac{1}{2} + \sqrt{\frac{2(1 - \rho^2)}{(\sigma/\sigma' + \sqrt{1 - \rho^2})^2 + (\sigma'/\sigma + \sqrt{1 - \rho^2})^2}}. \quad (31)$$

When $\theta = \pm\pi/4$, we have $\sigma = \sigma'$, and Eq. (31) becomes

$$F_{\text{pol.}}^{\text{max}} = \frac{1}{2} + \frac{\sqrt{1 - \rho^2}}{1 + \sqrt{1 - \rho^2}}. \quad (32)$$

Therefore, even with identical marginal spectra, the teleportation protocol is sensitive to the spectral entanglement between the polarization-entangled photon pair. This behavior contrasts with the results of the previous section, which found the two-photon polarization-correlation visibility, or equivalently, the concurrence, to become unity when $\sigma = \sigma'$, independent of the spectral entanglement, cf. Eq. (19).

For comparison, we also consider the joint probability amplitudes to be identical, i.e., $f(\omega, \omega') = g(\omega, \omega')$, such that the marginal spectra correlate with path. Then the overlap J is given by

$$J_{\text{path}} = \frac{2\sigma_1\sigma_M\sigma_m}{\sqrt{(\sigma_1^2\sigma'^2 + \sigma_M^2\sigma_m^2)(\sigma_1^2 + \sigma^2)}}. \quad (33)$$

or, equivalently,

$$J_{\text{path}} = \sqrt{\frac{4\sigma_1^2\sigma^2(1-\rho^2)}{(\sigma_1^2 + \sigma^2(1-\rho^2))(\sigma_1^2 + \sigma^2)}}. \quad (34)$$

Upon maximizing J_{path} with respect to σ_1 , we find the optimal bandwidth is given by $\sigma_1^4 = \sigma_M^2\sigma_m^2\sigma^2/\sigma'^2 = \sigma^4(1-\rho^2)$. The maximal obtainable fidelity is

$$F_{\text{path}}^{\text{max}} = \frac{1}{2} + \frac{2\sigma_M\sigma_m}{2\sigma_M\sigma_m + \sqrt{4\sigma_M^2\sigma_m^2 + (\sigma_M^2 - \sigma_m^2)^2 \sin^2 2\theta}}. \quad (35)$$

The results for $F_{\text{path}}^{\text{max}}$ are shown as the dashed lines in Fig. 4. When $a=1$, the fidelity is always unity because the joint spectrum is circularly symmetric and void of distinguishing information. However, very different behavior is observed for $a \neq 1$. Unit fidelity is obtained when $\theta=0$ and $\pm\pi/2$ because the joint spectrum is separable with respect to frequency. But rotating the spectrum decreases $F_{\text{path}}^{\text{max}}$ until a minimum is reached at $\theta=\pm\pi/4$. Here, the fidelities $F_{\text{path}}^{\text{max}}$ and $F_{\text{pol}}^{\text{max}}$ coincide because the two underlying relationships, Eqs. (3) and (5), are equivalent at this orientation. As in the previous case of $F_{\text{pol}}^{\text{max}}$, the diagonal orientation yields identical marginal bandwidths and a nonzero linear correlation $|\rho|=(a^2-1)/(a^2+1)$. As a increases, the photons become increasingly distinguishable with respect to frequency and the maximal value of $F_{\text{path}}^{\text{max}}$ approaches the classical limit of $1/2$. Finally, we note that $F_{\text{path}}^{\text{max}}$ can also be expressed in the relatively simple form

$$F_{\text{path}}^{\text{max}} = \frac{1}{2} + \frac{\sqrt{1-\rho^2}}{1 + \sqrt{1-\rho^2}}, \quad (36)$$

which is independent of the marginal bandwidths σ and σ' but depends on the spectral entanglement quantified by ρ .

V. CONCLUSIONS

We have analyzed both the polarization-correlation experiment and the quantum teleportation protocol using a multimode description of polarization-entangled photons. Our analysis accounted for the spectral entanglement carried by the joint amplitude accompanying the polarization-entangled photons, as well as the correlations between the spectral and polarization degrees of freedom. We found that in this broad bandwidth context, spectral entanglement between the photons reduces the maximal obtainable teleportation fidelity. This result contrasts with the behavior of the two-photon polarization-correlation visibility, which can be unity even when the photons are spectrally entangled.

The symmetry of the joint spectral amplitude has been found previously to affect entanglement-based experiments. U'Ren *et al.* [26] and Kim and Grice [27] have shown that the polarization-correlation visibility should always be maximal when $f(\omega, \omega')=g(\omega, \omega')$. We have extended these prior results by quantifying the visibility, or equivalently, the concurrence, for the case that the joint spectra are not identical. In particular, we have found that the visibility depends on the marginal spectra of the individual photons, as well as spectral entanglement between these photons.

We have also shown that maximizing polarization entanglement alone does not maximize the teleportation fidelity. Instead, one must also account for the distinguishing information provided by the spectral entanglement between the photons. This is evidenced by the family of dashed curves in Fig. 4 for which polarization entanglement is maximal, but the fidelity varies as a function of the spectral entanglement, cf. Eq. (36). An additional concern is the coupling between the spectral and polarization degrees of freedom, which, as seen from the family of solid curves in Fig. 4, leads to consistently lower fidelities.

Thus, in conclusion, the spectral degrees of freedom characterizing a polarization-encoded qubit have been shown to affect the quantum teleportation fidelity. These effects include both spectral entanglement between the photons and correlations between the spectral and the polarization degrees of freedom. We anticipate that the spatial modes characterizing single and biphoton states are similarly overlooked as sources of distinguishing information. Ongoing efforts to control these degrees of freedom during down conversion may eventually permit SPDC-based entanglement sources to be used for quantum teleportation without necessitating narrow-band spectral filters to guarantee the desired level of interference. We expect that success along this front will also benefit photonic implementations of other quantum information protocols.

ACKNOWLEDGMENTS

This paper describes activities performed under Contract No. DE-AC0500OR22750 between the U.S. Department of Energy and Oak Ridge Associated Universities. T.S.H. graciously acknowledges support from the Intelligence Community Research Program. This work was supported in part (W.P.G.) by the Disruptive Technology Office.

APPENDIX

Here we formalize our approximation to the joint spectral amplitude given in Eq. (7). In type-II SPDC, a pump pulse passes through a nonlinear optical crystal and generates (up to first order in perturbation theory) a pair of oppositely polarized photons [30]. With proper alignment of the emission cones, this setup prepares the two-photon state expressed by Eq. (1) [14]. For the case of a broad bandwidth pump pulse, the joint spectral amplitude f can be written as [18]

$$f(\omega, \omega') = \alpha(\omega + \omega')\Phi(\omega, \omega'), \quad (A1)$$

where $\alpha(\omega)$ is the pump-pulse spectrum centered about $2\omega_0$ and

$$\Phi(\omega, \omega') = \text{sinc}[\Delta\mathbf{k}(\omega, \omega') \cdot \hat{\mathbf{z}}L/2]e^{i\Delta\mathbf{k}(\omega, \omega') \cdot \hat{\mathbf{z}}L/2} \quad (A2)$$

is the phase-matching function and $\text{sinc}(x)=\text{sin}(x)/x$. The latter depends on the crystal length L and the mismatch

$$\Delta\mathbf{k}(\omega, \omega') = \mathbf{k}_p(\omega + \omega') - \mathbf{k}_o(\omega) - \mathbf{k}_e(\omega') \quad (A3)$$

between the wave vectors of the pump (p) and the ordinary (o) and extraordinary (e) rays. Recall that we have assumed

spatial filters define the paths that the down-converted photons take. When the beam waist of the pump pulse is small relative to the length of the crystal, additional terms coupling the spatial and spectral degrees of freedom enter the expression for the joint amplitude. See Refs. [26] for details. We assume here that the pump pulse is strictly collimated and that such coupling effects can be ignored.

In our approximation to Eq. (A1), we take the pump pulse to have a Gaussian spectrum centered at the mean frequency $2\omega_0$ with $(1/e)$ bandwidth σ_p . In addition, we expand the wave vector mismatch to first order in the difference frequencies $\Delta\omega = \omega - \omega_0$ and $\Delta\omega' = \omega' - \omega_0$, and we assume that down conversion is phase matched at zero order in this expansion. Then, the probability amplitude is approximated by

$$f(\Delta\omega, \Delta\omega') \cong N \exp[-(\Delta\omega + \Delta\omega')^2/2\sigma_p^2 - \gamma(\tau_o\Delta\omega + \tau_e\Delta\omega')^2/2 + i(\tau_o\Delta\omega + \tau_e\Delta\omega')], \quad (\text{A4})$$

where the times $\tau_o = L[k'_p(2\omega_0) - k'_o(\omega_0)]$ and $\tau_e = L[k'_p(2\omega_0) - k'_e(\omega_0)]$ are the differences in transit times through the crystal between the pump and the o and e rays, respectively, and the prefactor $N^4 = \gamma|\tau_o - \tau_e|^2/\pi\sigma_p^2$ is a normalization constant. The constant γ is chosen to match the full width half maxi-

mum (FWHM) of a Gaussian envelope to the modulus of the phase-matching function; the overlap of $\text{sinc}(x/2)$ and a FWHM-matched Gaussian envelope $\exp(-\gamma x^2)$ is ~ 0.94 for the chosen value of $\gamma \cong 0.04823$.

We rewrite Eq. (A4) as the normal distribution given by Eq. (7), with the following definitions for the marginal bandwidths,

$$\begin{aligned} \sigma^2 &= (1 + \gamma\tau_e^2\sigma_p^2)/\gamma|\tau_o - \tau_e|^2, \\ \sigma'^2 &= (1 + \gamma\tau_o^2\sigma_p^2)/\gamma|\tau_o - \tau_e|^2, \end{aligned} \quad (\text{A5})$$

and the linear correlation

$$\rho = -(1 + \gamma\tau_o\tau_e\sigma_p^2)/\sqrt{(1 + \gamma\tau_o^2\sigma_p^2)(1 + \gamma\tau_e^2\sigma_p^2)}. \quad (\text{A6})$$

Note that in the limit of vanishing pump-pulse bandwidth (the cw-pump case), the correlation approaches -1 [34]. Finally, although distinguishing information is potentially contained in both the modulus and the phase of the probability amplitude, we neglect the latter in our analysis, instead assuming that linear phase effects can be accounted for by using a compensating crystal in one of the output arms [35].

-
- [1] C. H. Bennett, G. Brassard, C. Crépeau, R. Jozsa, A. Peres, and W. K. Wootters, *Phys. Rev. Lett.* **70**, 1895 (1993).
- [2] M. A. Nielsen and I. L. Chuang, *Quantum Computation and Quantum Information* (Cambridge, New York, 2000).
- [3] H.-J. Briegel, W. Dür, J. I. Cirac, and P. Zoller, *Phys. Rev. Lett.* **81**, 5932 (1998).
- [4] B. C. Jacobs, T. B. Pittman, and J. D. Franson, *Phys. Rev. A* **66**, 052307 (2002).
- [5] H. de Riedmatten, I. Marcikic, W. Tittel, H. Zbinden, D. Collins, and N. Gisin, *Phys. Rev. Lett.* **92**, 047904 (2004).
- [6] B. Julsgaard, J. Sherson, J. I. Cirac, J. Fiurášek, and E. S. Polzik, *Nature (London)* **432**, 482 (2004).
- [7] E. Knill, R. Laflamme, and G. J. Milburn, *Nature (London)* **409**, 46 (2001).
- [8] D. Bouwmeester, J.-W. Pan, K. Mattle, M. Eibl, H. Weinfurter, and A. Zeilinger, *Nature (London)* **390**, 575 (1997).
- [9] Y.-H. Kim, S. P. Kulik, and Y. Shih, *Phys. Rev. Lett.* **86**, 1370 (2001).
- [10] J.-W. Pan, M. Daniell, S. Gasparoni, G. Weihs, and A. Zeilinger, *Phys. Rev. Lett.* **86**, 4435 (2001).
- [11] T. Jennewein, G. Weihs, J.-W. Pan, and A. Zeilinger, *Phys. Rev. Lett.* **88**, 017903 (2002).
- [12] J.-W. Pan, S. Gasparoni, M. Aspelmeyer, T. Jennewein, and A. Zeilinger, *Nature (London)* **421**, 721 (2003).
- [13] R. Ursin, T. Jennewein, M. Aspelmeyer, R. Kaltenbaek, M. Lindenthal, P. Walther, and A. Zeilinger, *Nature (London)* **430**, 849 (2004).
- [14] P. G. Kwiat, K. Mattle, H. Weinfurter, A. Zeilinger, A. V. Sergienko, and Y. Shih, *Phys. Rev. Lett.* **75**, 4337 (1995).
- [15] P. G. Kwiat, E. Waks, A. G. White, I. Appelbaum, and P. H. Eberhard, *Phys. Rev. A* **60**, R773 (1999).
- [16] S. L. Braunstein and A. Mann, *Phys. Rev. A* **51**, R1727 (1995).
- [17] T. E. Keller and M. H. Rubin, *Phys. Rev. A* **56**, 1534 (1997).
- [18] W. P. Grice and I. A. Walmsley, *Phys. Rev. A* **56**, 1627 (1997).
- [19] Y. H. Kim, S. P. Kulik, M. V. Chekhova, W. P. Grice, and Y. Shih, *Phys. Rev. A* **67**, 010301(R) (2003).
- [20] G. Di Giuseppe, L. Haiberger, F. De Martini, and A. V. Sergienko, *Phys. Rev. A* **56**, R21 (1997).
- [21] W. P. Grice, R. Erdmann, I. A. Walmsley, and D. Branning, *Phys. Rev. A* **57**, R2289 (1998).
- [22] D. Branning, W. Grice, R. Erdmann, and I. A. Walmsley, *Phys. Rev. A* **62**, 013814 (2000).
- [23] C. K. Hong, Z. Y. Ou, and L. Mandel, *Phys. Rev. Lett.* **59**, 2044 (1987).
- [24] S. P. Walborn, A. N. de Oliveira, S. Pádua, and C. H. Monken, *Phys. Rev. Lett.* **90**, 143601 (2003).
- [25] C. K. Law and J. H. Eberly, *Phys. Rev. Lett.* **92**, 127903 (2004).
- [26] A. B. U'Ren, E. Mukamel, K. Banaszek, and I. A. Walmsley, *Philos. Trans. R. Soc. London, Ser. A* **361**, 1493 (2003); A. B. U'Ren, K. Banaszek, and I. A. Walmsley, *Quantum Inf. Comput.* **3**, 480 (2003).
- [27] Y.-H. Kim and W. P. Grice, *Phys. Rev. A* **68**, 062305 (2003).
- [28] P. P. Rohde and T. C. Ralph, *Phys. Rev. A* **71**, 032320 (2005).
- [29] P. P. Rohde, T. C. Ralph, and M. A. Nielsen, *Phys. Rev. A* **72**, 052332 (2005).
- [30] D. C. Burnham and D. L. Weinberg, *Phys. Rev. Lett.* **25**, 84 (1970).
- [31] W. K. Wootters, *Phys. Rev. Lett.* **80**, 2245 (1998).
- [32] N. Lütkenhaus, J. Calsamiglia, and K.-A. Suominen, *Phys. Rev. A* **59**, 3295 (1999).
- [33] Rohde and Ralph provide a comprehensive model for the photodetectors used in a quantum optics experiment that is capable

of accounting for not only finite spectral resolution but also dark counts, dead time, and nonunit detector efficiency. See P. P. Rohde and T. C. Ralph, *J. Mod. Opt.* **53**, 1589 (2006).

[34] The extent to which the spectral entanglement can be modified by controlling the parameters of the experiment has been in-

vestigated previously; see W. P. Grice, A. B. U'Ren, and I. A. Walmsley, *Phys. Rev. A* **64**, 063815 (2001); U'Ren *et al.*, *Laser Phys.* **15**, 146 (2005); and Ref. [26].

[35] R. Erdmann, D. Branning, W. Grice, and I. A. Walmsley, *Phys. Rev. A* **62**, 053810 (2000).